Available online at www.sciencedirect.com
SCIENCE DIRECT®
Journal of Sound and Vibration 288 (2005) 255–273
JOURNAL OF SOUND AND VIBRATION
www.elsevier.com/locate/jsvi

Acoustic modelling and testing of diesel particulate filters

Sabry Allam, Mats Åbom*

The Marcus Wallenberg Laboratory for Sound and Vibration Research, Department of Aeronautical and Vehicle Engineering, KTH, SE-10044 Stockholm, Sweden

Received 6 July 2004; received in revised form 20 December 2004; accepted 7 January 2005
Available online 8 March 2005

Abstract

The use of Diesel Particulate Filters (DPFs) on automobiles to reduce the harmful effects of diesel exhaust gases is becoming a standard in many countries. Although the main purpose of a DPF is to reduce harmful emission of soot particles it also affects the acoustic emission. This paper presents a first attempt to describe the acoustic behavior of DPFs and to present models which allow the acoustic two-port to be calculated. The simplest model neglects wave propagation and treats the filter as an equivalent acoustic resistance modeled via a lumped impedance element. This simple model gives a constant frequency-independent transmission loss and agrees within 1 dB with measured data on a typical filter (length 250 mm) up to 200–300 Hz (at 20 °C). In the second model, the ceramic filter monolith is described as a system of coupled porous channels carrying plane waves. The coupling between the channels through the porous walls is described via Darcy's law. This model gives a frequency-dependent transmission loss and agrees well with measured data in the entire plane wave range.

1. Introduction

The continuous growth of diesel engines in the market has put focus on the environmental effects and in particular on methods to reduce the soot particle emission. An ambitious way to diesel particulate removal is the use of a particulate trap that allows simultaneous soot filtration and combustion, see Fig. 1.

*Corresponding author. Tel.: +46 8 790 7944; fax: +46 8 790 6122.
E-mail address: matsabom@kth.se (M. Åbom).

0022-460X/$ - see front matter © 2005 Elsevier Ltd. All rights reserved.
doi:10.1016/j.jsv.2005.01.004

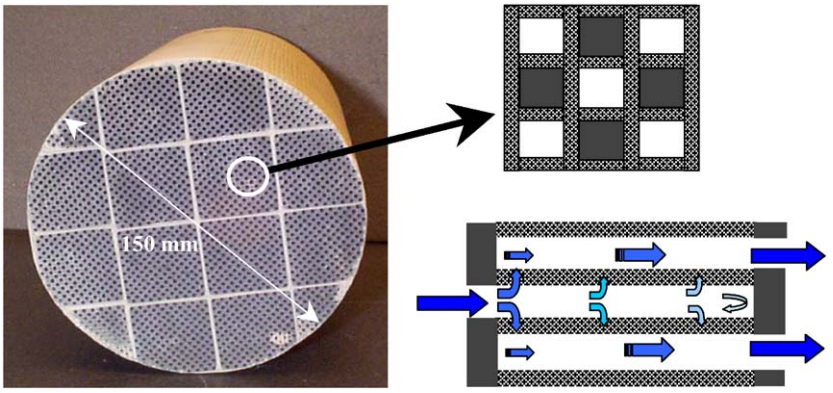

Fig. 1. Photograph of a typical ceramic diesel particulate filter unit with illustration of the flow path through the filter. The flow enters one channel plugged at the downstream end and then passes through the porous walls into the four neighboring channels plugged at the upstream end. At the inlet side of the filter close to 50% of the channels are plugged. A typical width of the square channels is 1–2 mm with a wall thickness of a few tenths of a millimeter.

The particulate trap concept has focused intensive research and development activities around the world and a variety of systems are today offered by various manufactures. Among the possible filter types, ceramic foams seem to be the best, especially to meet the requirements of efficient filtration. Two parameters are of key importance when investigating the effect of a trap system on a diesel engine [1]: back-pressure and regeneration. The back-pressure is different for different types of traps and will increase over time as the trap becomes loaded with particles. A high back-pressure is undesirable, since it increases the fuel consumption and reduces the available power. Minimizing the back-pressure level while still maintaining acceptable filtration efficiency and meeting other constraints is the major challenge when designing particulate traps.

Linked to the back-pressure is the removal of soot by trap regeneration. For typical engine operating conditions this regeneration needs to take place each 500–1000 km. Various strategies exist for regeneration but normally the soot layer and back-pressure is allowed to grow to a certain limit, then a regeneration cycle which burns the particles and cleans the trap is initiated. A significant number of publications exist on back-pressure and regeneration for DPF units, see e.g., Konstandopoulos and Johnson [2], Konstandopoulos et al. [3] and Masoudi et al. [4].

2. Theory

No previous works on the acoustic modeling of diesel particulate filters seem to exist. But a summary of the models presented here has been presented earlier by Allam and Åbom [5]. The purpose of this section is to present two models, a simple one, valid for low frequencies and a more detailed one, valid in the entire plane wave range. Using the models expressions for the acoustic two-port of a diesel particulate fitters (DPF) unit will be derived. The proposed models are based on the following assumptions:

(i) Only plane (1-D) acoustic waves are considered,
(ii) Linear acoustics is valid,

(iii) The Mach number (M) is small (<0.1),
(iv) Gradients (temperature, mean flow speed) in the axial direction are neglected,
(v) The effects of chemical reactions are neglected.

Comments:

(i) For the application to automobile exhaust systems analysis in the low-frequency plane wave range is normally sufficient.
(ii) The DPF is close to the manifold junction where the first engine harmonics can have levels up to 160–170 dB. The frequency of these dominating harmonics is low (less than 100 Hz) so the shock formation distance is typically much longer than the length of the exhaust system. Furthermore, for open ended systems as exhaust systems, wave steepening effects are weakened by successive reflections at sudden area expansions where the reflection coefficient is negative [6]. Therefore, under steady (non-transient) running conditions for an engine nonlinear wave propagation effects are of minor importance, instead local nonlinearities associated with flow separation at constrictions (small holes) dominate. Such local nonlinear effects are related to the turbulent (quadratic) pressure drop for an element. For DPF units at hot conditions laminar flow conditions dominate and the quadratic pressure drop contribution is very small (see Section 3.2), which implies that local nonlinearities should be weak.
(iii) To reduce the back-pressure a DPF is normally placed in an expansion chamber so that the mean flow speed is reduced. Typically the reduction is of the order of 10 which is reduced to a factor 3–5 due to the contraction when the flow enters the filter. Since the Mach number in an exhaust system normally is less than 0.3 this implies that $M<0.1$.
(iv) Gradients will exist but a constant (= average) value for the mean flow speed and the temperature (speed of sound) will be shown to be a good approximation.
(v) Chemical reactions (the burning of soot) will mainly occur during the regeneration of a filter.

2.1. The lumped impedance model

In this model wave propagation is neglected and the filter is simply treated as an acoustic resistance. The model will be valid in the low-frequency range where the wavelength is much larger than the length of a filter unit. Typically for an automobile filter this means up to 200–300 Hz at cold conditions (20 °C) and 400–600 Hz under operating conditions (500 °C).

To obtain the acoustic resistance it is assumed that the acoustic field acts as a quasi-stationary disturbance of the pressure-drop over the filter unit. As described in the literature the steady flow pressure-drop ΔP over a DPF follows Darcy's law with Forchheimer's extension [7] and can be described as

$$\Delta P = R_1 U_0 + R_2 U_0^2, \tag{1}$$

where U_0 is the flow speed, R_1 is equal to the linear "viscous" flow resistance and R_2 is the quadratic flow resistance. Differentiating this equation gives

$$\mathrm{d}(\Delta P) = \left(\frac{R_1 + 2R_2 U_0}{A}\right) \mathrm{d}Q, \tag{2}$$

where $dQ = dU_0 A$ is volume flow and A the filter cross-sectional area. Eq. (2) implies that the acoustic resistance R_{ac} is given by

$$R_{ac} = \left(\frac{R_1 + 2R_2 U_0}{A}\right). \tag{3}$$

Since the Mach number in the filter is small ($M < 0.1$) continuity of volume flow can be assumed and the two-port (in transfer matrix form) for a lumped resistance model becomes

$$\begin{pmatrix} p \\ q \end{pmatrix}_{IN} = \begin{pmatrix} 1 & R_{ac} \\ 0 & 1 \end{pmatrix} \begin{pmatrix} p \\ q \end{pmatrix}_{OUT}, \tag{4}$$

where p is acoustic pressure, q acoustic volume velocity and (IN, OUT) denote the inlet and outlet of the filter.

2.2. The 1-D wave model

With reference to Fig. 2 a unit cell in a filter can be split into 5 sections: the inlet cross-section (IN), a short narrow pipe with hard impermeable walls (I); the filter section consisting of narrow pipes with porous walls (II); a short narrow pipe with hard impermeable walls (III) and the outlet cross-section (OUT). In the plane wave range these sections can be described via two-port transfer matrices (**T**). The resulting transfer matrix for a filter unit is then simply

$$\mathbf{T}_{DPF} = \mathbf{T}_{IN}\mathbf{T}_{I}\mathbf{T}_{II}\mathbf{T}_{III}\mathbf{T}_{OUT}. \tag{5}$$

2.2.1. The filter section (II)

The governing equations for acoustic waves can be derived by linearizing the 1-D fluid dynamic equations for a DPF presented in Ref. [2]. Assuming a homogenous mean flow and ambient state this gives for the equation of continuity

$$\frac{\partial \rho_j}{\partial t} + U_{oj}\frac{\partial \rho_j}{\partial x} + \rho_{oj}\frac{\partial u_j}{\partial x} = (-1)^j \frac{4\rho_w}{d_{hj}} u_w, \tag{6}$$

and the equation of momentum

$$\rho_{oj}\left(\frac{\partial}{\partial t} + U_{oj}\frac{\partial}{\partial x}\right)u_j = -\frac{\partial p_j}{\partial x} - \alpha_j u_j. \tag{7}$$

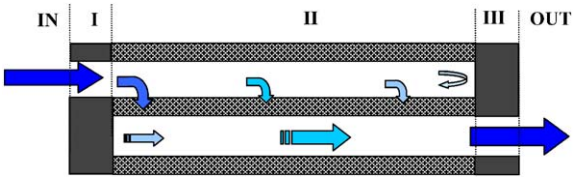

Fig. 2. Cross-section of a unit cell in a DPF split into five sections each described by an acoustic two-port. Note, the filter section (II) is actually an acoustic four-port but can be reduced to a two-port due to the hard walls in section I and III.

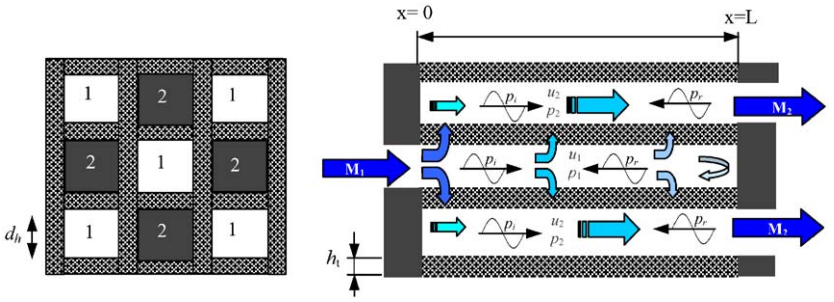

Fig. 3. Neighboring channels in a DPF unit. The flow and the acoustic waves enter the channels (1) open upstream and closed downstream, then pass through the porous walls into the channels (2) closed upstream and open downstream.

Here $j = 1, 2$ denotes the inflow (1) and outflow channel (2), see Fig. 3, ρ_o and U_o denote the time average density and axial flow speed, and u, ρ, p denote the fluctuation in axial particle velocity, density, and pressure, u_w is the particle velocity fluctuation through the wall, ρ_w is the gas density in the porous wall and d_h is the width of the quadratic channels. In the limit of very narrow channels and low frequencies, laminar flow can be assumed and the pressure drop factor will be $\alpha = \mu\varepsilon/d_h^2$, where μ is the dynamic viscosity and ε is the channel pressure drop factor. Since the local flow passing through the walls is only a small fraction of the total axial mean flow, the velocity profile should be close to that observed for laminar flow in a quadratic duct with impermeable walls which implies $\varepsilon = 28.45$ [2,4].

The coupling between the fields in channels 1 and 2 is via the porous walls. Since these walls are very thin the steady-state flow resistance (Darcy's law) will apply also to the fluctuating acoustic fields [8]. A constant (frequency-independent) wall resistance can therefore be defined as

$$R_w = (p_1 - p_2)/u_w. \tag{8}$$

This wall resistance can be linked to the properties of the porous wall and the gas [2–4] by

$$R_w = \frac{\mu_w h_t}{\sigma_w}, \tag{9}$$

where μ_w is the dynamic viscosity, h_t thickness and σ_w is the permeability of the wall.

To solve the problem a propagating wave ansatz is made and harmonic space and time dependence introduced. Suppressing the harmonic time dependence ($e^{i\omega t}$) the fluctuating quantities can then be written as

$$\begin{aligned} &p_j(x) = \hat{p}_j e^{-iKx}, \quad u_j(x) = \hat{u}_j e^{-iKx}, \\ &\hat{p}_j = c_j^2 \hat{\rho}_j, \\ &\hat{p}_j = Z_j \hat{u}_j, \end{aligned} \tag{10}$$

where tilde denotes complex amplitude, K is the complex wavenumber, c is the speed of sound and Z is the characteristic wave impedance. Substituting Eqs. (8) and (10) into Eqs. (6)

and (7) gives

$$\frac{\mathrm{i}\omega}{c_j^2}\hat{p}_j + \frac{U_{oj}}{c_j^2}(-\mathrm{i}K)\hat{p}_j + \rho_{oj}Z_j^{-1}\hat{p}_j(-\mathrm{i}K) = (-1)^j\frac{4\rho_w}{d_{hj}R_w}(\hat{p}_1 - \hat{p}_2), \tag{11}$$

$$\rho_{oj}(\mathrm{i}\omega + U_{oj}(-\mathrm{i}K))Z_j^{-1} = \mathrm{i}K - \alpha_j Z_j^{-1}. \tag{12}$$

From Eq. (12) the characteristic wave impedance can be obtained

$$Z_j = \frac{\rho_{oj}\omega - \mathrm{i}\alpha_j - \rho_{oj}U_{oj}K}{K} = \frac{\rho_{oj}c_j(k_j' - M_jK)}{K}, \tag{13}$$

where $M_j = U_{oj}/c_j$, $k_j' = k_j - \mathrm{i}\alpha_j/\rho_{oj}c_j$ and $k_j = \omega/c_j$. Substituting Eq. (13) into Eq. (11) gives

$$\left(\frac{\mathrm{i}k_j}{c_j}\right)\hat{p}_j - \left(\frac{\mathrm{i}M_jK}{c_j}\right)\hat{p}_j - \frac{\mathrm{i}K^2}{c_j(k_j' - M_jK)}\hat{p}_j = (-1)^j\frac{4\rho_w}{d_{hj}R_w}(\hat{p}_1 - \hat{p}_2). \tag{14}$$

Multiplying this by i, c_j and putting $B_j = c_j\rho_w/d_{hj}R_w$ finally gives

$$-(k_j - M_jK)\hat{p}_j + \frac{K^2}{(k_j' - M_jK)}\hat{p}_j = (-1)^j 4\mathrm{i}B_j(\hat{p}_1 - \hat{p}_2). \tag{15}$$

Eq. (15) represents a pair of homogenous linear equations which have non-trivial solutions (eigenvalues) for the wavenumbers K corresponding to free waves in the porous channels. This linear equation system can be written as

$$\begin{pmatrix} K_1^2 + 4\mathrm{i}B_1(k_1' - M_1K) & -4\mathrm{i}B_1(k_1' - M_1K) \\ -4\mathrm{i}B_2(k_2' - M_2K) & K_2^2 + 4\mathrm{i}B_2(k_2' - M_2K) \end{pmatrix}\begin{pmatrix} \hat{p}_1 \\ \hat{p}_2 \end{pmatrix} = \begin{pmatrix} 0 \\ 0 \end{pmatrix}, \tag{16}$$

where $K_j^2 = K^2 - (k_j - M_jK)(k_j' - M_jK)$. Eq. (16) defines a fourth-order algebraic equation for the wavenumbers K_n, $n = 1, 2, 3, 4$. To each of the wavenumbers there is a corresponding 2-D mode (eigenvector) $\mathbf{e}_n$. The eigenvalues and corresponding modes can be calculated numerically for instance by using Matlab. Using these eigenvalues and modes a general expression for the sound field in the filter section can be written as

$$\begin{pmatrix} \hat{p}_1(x) \\ \hat{p}_2(x) \end{pmatrix} = \sum_{n=1}^{4} \hat{a}_n \mathrm{e}^{-\mathrm{i}K_n x}\mathbf{e}_n, \tag{17}$$

where $\hat{a}_n$ are the modal amplitudes. From this equation the acoustic volume flows can be obtained by division by the characteristic wave impedance Z_j and multiplication with the cross-sectional area d_{hj}^2 of the channels

$$\begin{pmatrix} \hat{q}_1(x) \\ \hat{q}_2(x) \end{pmatrix} = \sum_{n=1}^{4} \hat{a}_n \mathrm{e}^{-\mathrm{i}K_n x}\mathbf{e}_n', \tag{18}$$

where $e_{j,n}' = e_{j,n}d_{hj}^2/Z_{j,n}$. Eqs. (17) and (18) will now be used to obtain the acoustic four-port in transfer matrix form for the filter section. First the following relationship between p and q and

modal amplitudes can be written down

$$\begin{pmatrix} \hat{p}_1(x) \\ \hat{p}_2(x) \\ \hat{q}_1(x) \\ \hat{q}_2(x) \end{pmatrix} = \begin{pmatrix} e^{-iK_1x}\mathbf{e}_1 & e^{-iK_2x}\mathbf{e}_2 & e^{-iK_3x}\mathbf{e}_3 & e^{-iK_4x}\mathbf{e}_4 \\ e^{-iK_1x}\mathbf{e}'_1 & e^{-iK_2x}\mathbf{e}'_2 & e^{-iK_3x}\mathbf{e}'_3 & e^{-iK_4x}\mathbf{e}'_4 \end{pmatrix} \begin{pmatrix} \hat{a}_1 \\ \hat{a}_2 \\ \hat{a}_3 \\ \hat{a}_4 \end{pmatrix}. \tag{19}$$

Denoting the 4×4 matrix in Eq. (19) by $\mathbf{H}(x)$ and applying this equation to $x = 0$ and $x = L$ gives

$$\begin{pmatrix} \hat{p}_1(0) \\ \hat{p}_2(0) \\ \hat{q}_1(0) \\ \hat{q}_2(0) \end{pmatrix} = \mathbf{H}(0) \begin{pmatrix} \hat{a}_1 \\ \hat{a}_2 \\ \hat{a}_3 \\ \hat{a}_4 \end{pmatrix} \quad \text{and} \quad \begin{pmatrix} \hat{p}_1(L) \\ \hat{p}_2(L) \\ \hat{q}_1(L) \\ \hat{q}_2(L) \end{pmatrix} = \mathbf{H}(L) \begin{pmatrix} \hat{a}_1 \\ \hat{a}_2 \\ \hat{a}_3 \\ \hat{a}_4 \end{pmatrix}.$$

Solving the modal amplitudes from the second of these equations and putting the result into the first gives

$$\begin{pmatrix} \hat{p}_1(0) \\ \hat{p}_2(0) \\ \hat{q}_1(0) \\ \hat{q}_2(0) \end{pmatrix} = \mathbf{H}(0)\mathbf{H}^{-1}(L) \begin{pmatrix} \hat{p}_1(L) \\ \hat{p}_2(L) \\ \hat{q}_1(L) \\ \hat{q}_2(L) \end{pmatrix}. \tag{20}$$

The four-port matrix ($\mathbf{S} = \mathbf{H}(0)\mathbf{H}^{-1}(L)$) in Eq. (20) can be reduced to a two-port matrix $\mathbf{T}$ by using the rigid wall boundary conditions in channel 1 and 2, i.e., $\hat{q}_2(0) = 0$ and $\hat{q}_1(L) = 0$. A straightforward derivation reveals that

$$\begin{pmatrix} \hat{p}_1(0) \\ \hat{q}_1(0) \end{pmatrix} = \mathbf{T} \begin{pmatrix} \hat{p}_2(L) \\ \hat{q}_2(L) \end{pmatrix} \quad \text{with } \mathbf{T} = \begin{pmatrix} S_{12} - S_{42}S_{11}/S_{41} & S_{14} - S_{44}S_{11}/S_{41} \\ S_{32} - S_{42}S_{31}/S_{41} & S_{34} - S_{44}S_{31}/S_{41} \end{pmatrix}. \tag{21}$$

To obtain the total acoustic volume flow all the open channels (N) at the inlet ($x = 0$) and the outlet ($x = L$) should be added. The volume flows in Eq. (21) should therefore be multiplied by N, which implies that the two-port matrix $\mathbf{T}_{\mathrm{II}}$ for the entire filter section (including all channels) is related to the $\mathbf{T}$-matrix in Eq. (21)

$$\mathbf{T}_{\mathrm{II}} = \begin{pmatrix} T_{11} & T_{12}/N \\ NT_{21} & T_{22} \end{pmatrix}. \tag{22}$$

2.2.1.1. The no flow case. Since the Mach number is small in the filter section (<0.1) it seems a good approximation would be to put it to zero in the acoustic model. An analytical solution of the eigenvalue problem is then possible. Considering the tests of clean filters at room temperature presented later, the cross-section and speed of sound will also be assumed constant in the filter.

With these simplifications the wavenumbers and eigenvectors become

$$\begin{cases} K_1 = -K_2 = k, \\ K_3 = -K_4 = k\sqrt{1 - 8\mathrm{i}B/k}, \end{cases} \quad \begin{cases} \mathbf{e}_1 = \mathbf{e}_2 = \begin{pmatrix} 1 \\ 1 \end{pmatrix}, \\ \mathbf{e}_3 = \mathbf{e}_4 = \begin{pmatrix} 1 \\ -1 \end{pmatrix}. \end{cases} \tag{23}$$

This case can also serve as a validation case for the coded version of the general model.

2.2.1.2. Choice of speed of sound. To use the 1-D wave model values for the speed of sound (c) and damping (α) must be supplied. For sound propagation in ducts there exist two asymptotic cases: (i) low frequencies or narrow ducts; (ii) high frequencies or wide ducts [8]. In case (i) viscous effects dominate and the speed of sound should be put equal to the isothermal sound speed and α is related to the pressure drop for a laminar flow profile (see Eq. (7)). For case (ii) the adiabatic sound speed applies and a frequency-dependent damping should be added. This can be done by dropping α from the equation of motion and instead adding a term $(1 - \mathrm{i})\alpha_j$ to the wavenumbers k_j, where α corresponds to the classical Kirchhoff value for acoustic damping in pipes [8]. Typical cross dimensions for the channels in a DPF are 1–2 mm. This should be compared with the thickness of the viscous/thermal acoustic boundary layers, which for air at 20 °C and normal pressure is around 0.2 mm at 100 Hz. The low-frequency (case (i)) approximation will be valid when the acoustic boundary layers have fully merged and at cold conditions this will only be true for very low frequencies. Therefore for filters tested at room temperature the approximation obtained by using case (ii) is probably the better choice. But for filters at typical operating temperatures (500–700 °C) the boundary layers will be significantly thicker (a factor 2.5) and then case (i) is probably the best choice.

2.2.2. The complete filter model

With reference to Fig. 2 and Eq. (5) two-port models are also needed for the in- and outlet sections plus the short straight pipe sections (I and III). Concerning the straight pipe sections these can be modeled using standard models from the literature for narrow pipes with flow. However, since the length of these pipes is less than 1 cm it is possible to simply add them as an end correction (mass plug) to the in- and outlet sections. The in- and outlet sections represent an area constriction and expansion, respectively, where both acoustic and flow near fields can influence the plane wave transmission. A number of models for acoustic transmission at area changes exist [9–11], but for low frequencies and small Mach numbers a simple lumped impedance model can be used. This implies a two-port of the following form:

$$\mathbf{T}_X = \begin{pmatrix} 1 & Z_X \\ 0 & 1 \end{pmatrix}, \tag{24}$$

where X denotes sections IN + I or sections III + OUT and the impedance is calculated from

$$Z_X = r_X + \frac{\mathrm{i}\rho_X \omega l_X}{d_{hj}^2 N}. \tag{25}$$

Here r is the acoustic resistance which depends on viscous and flow related losses and l is the end correction. In the results presented later the viscous contribution to r will be neglected and the flow related (''turbulent'') losses will be determined from the quadratic term in Darcy's law. Concerning the end correction it will be put equal to the lengths of sections I and III since the contribution from the openings are much smaller.

Once all the matrices are determined for a filter unit the total two-port is calculated from Eq. (5). The filter transmission losses can then be obtained from Ref. [10]

$$TL = 10\log_{10}\left\{\left(\frac{1+M_{\text{in}}}{1+M_{\text{out}}}\right)^2 \frac{Z_{\text{in}}}{4Z_{\text{out}}}\left|T_{11}^{\text{DPF}} + \frac{T_{12}^{\text{DPF}}}{Z_{\text{out}}} + Z_{\text{in}}T_{21}^{\text{DPF}} + \frac{Z_{\text{in}}T_{22}^{\text{DPF}}}{Z_{\text{out}}}\right|^2\right\}, \tag{26}$$

where M_{in}, M_{out} and Z_{in}, Z_{out} are the Mach numbers and the acoustic impedance at the in- and outlet of the filter.

2.2.3. Temperature and mean-flow gradients

In the model presented above gradients in temperature and mean flow are neglected. For real cases it is necessary to include such effects and it will be assumed that this can be done by splitting the filter section into cells with piecewise constant states approximating the continuous variation. The length of each constant state cell is chosen so that it is much smaller than the wavelength at the highest frequency of interest. For each cell the four-pole matrix is calculated using the theory presented above. The four-pole matrices for all cells are then multiplied to obtain the matrix for the entire filter section. This is then reduced to a two-port as described above.

2.3. Predicted damping for a DPF at operating conditions

To investigate the predictions resulting from the models a typical DPF unit has been analyzed. The data used for the calculations are summarized in Table 1.

For the fluid state at the inlet of the unit the following data are assumed: Temperature 700 °K, static pressure 1.0E5 Pa and Mach number 0.020. The fluid is assumed to be an ideal gas (air) and standard formulas for the temperature dependence of sound speed and viscosity were used [8]. To obtain the mean flow and temperature distribution corresponding to real DPF units the data and the models in Refs. [2,3] were used. The results for a clean filter and a filter with soot loading are shown in Figs. 4–7. Concerning the soot loading a thickness of $\frac{1}{10}$ of the wall thickness was assumed and a permeability of $\sigma_{\text{soot}} = 1.5 \times 10^{-14}$. The resulting wall resistance with soot loading

Table 1
Data for the studied DPF

Diameter/length (mm)	$n \times 10^{-5}$ (channels/m^2)	Channel width $d_h \times 10^3$ (m)	Wall thickness $h_t \times 10^4$ (m)	Wall permeability $\sigma_w \times 10^{13}$ (m^2)
150/250	3.10	1.44	3.55	2.50

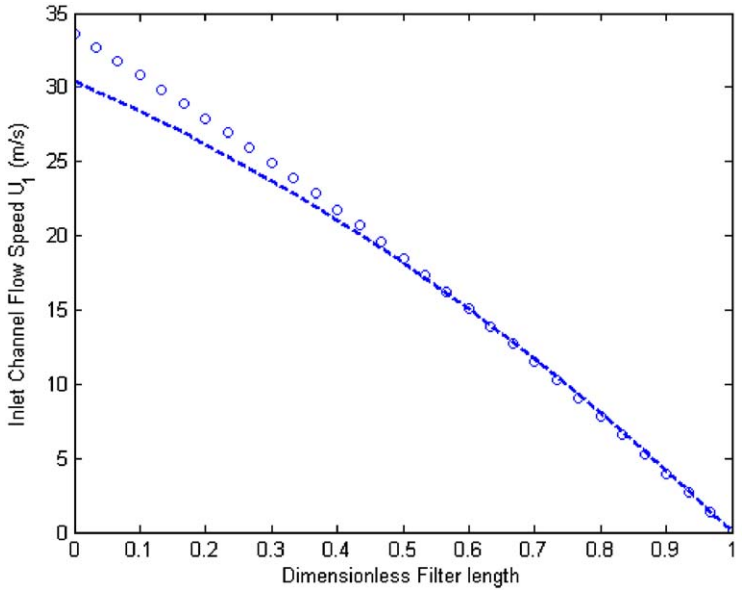

Fig. 4. Inlet channel flow speed distribution in the studied DPF unit. ○ ○ ○, with soot layers; - - - -, without soot layers.

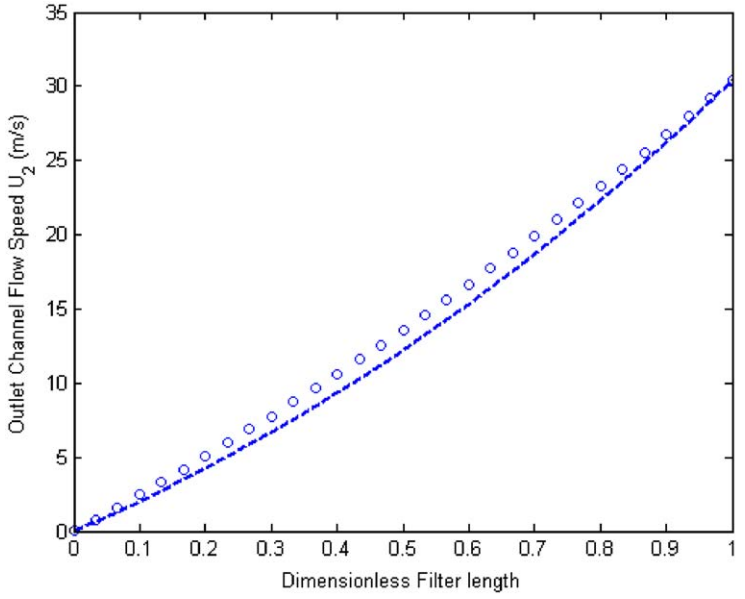

Fig. 5. Outlet channel flow speed distribution in the studied DPF unit. ○ ○ ○, with soot layers; - - - -, without soot layers.

added is given by [2,4]

$$R_w = \mu_w \left(\frac{h_t}{\sigma_w} + \frac{h_{\text{soot}}}{\sigma_{\text{soot}}} \right). \tag{27}$$

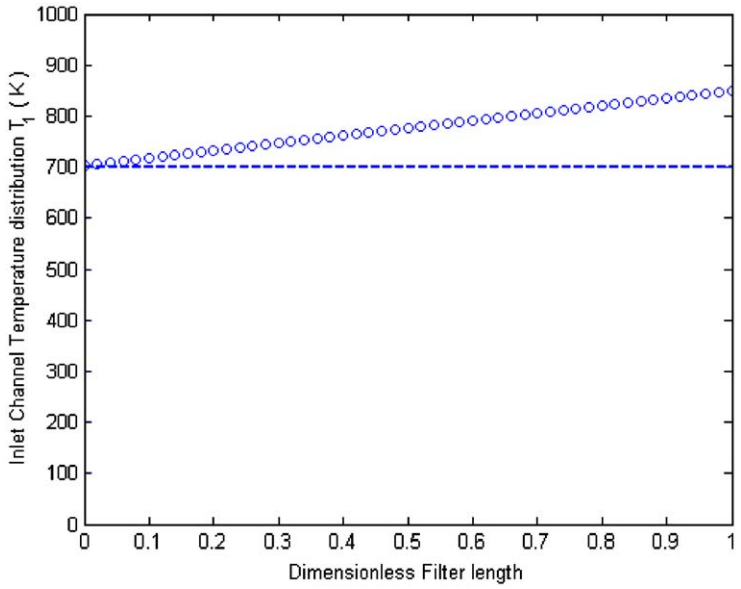

Fig. 6. Inlet channel temperature distribution in the studied DPF unit. ○ ○ ○, with soot layers; - - - -, without soot layers.

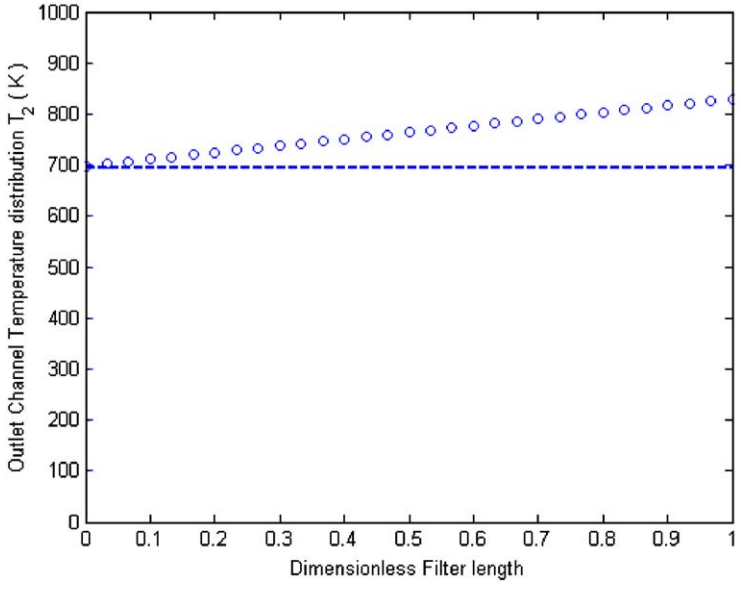

Fig. 7. Outlet channel temperature distribution in the studied DPF unit. ○ ○ ○, with soot layers; - - - -, without soot layers.

where σ_w is the ceramic wall permeability. The chosen thickness of the soot layer corresponds to a value typical for the state just before filter regeneration would start.

Using the 1-D wave model the transmission loss has been calculated for the filter defined in Table 1 for a Mach number of 0.020 in the inlet duct. For the sound propagation in the channels it

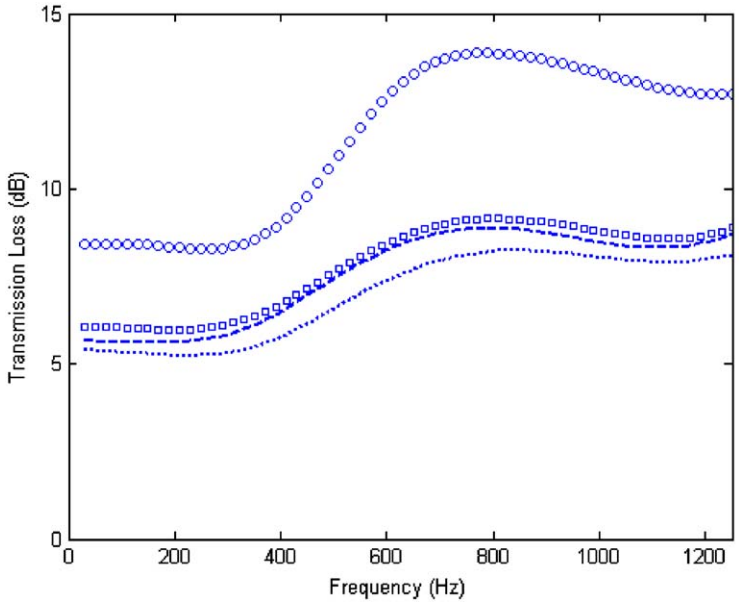

Fig. 8. Predicted transmission loss for the studied filter unit at $M = 0.02$ and $T = 700\,^{\circ}\mathrm{K}$ before the filter inlet. ...., Predicted for no flow and no soot; □ □ □, predicted for no flow in the channels and no soot BUT with flow losses at the inlet/outlet; ----, predicted with flow and no soot ; ○ ○ ○, predicted with flow and soot layer.

is assumed that case (i) holds, i.e., isothermal speed of sound and fully merged acoustic boundary layers (see Section 2.2.1.2). The results are shown in Fig. 8. As can be seen from the three clean filter curves, the effect of mean-flow convection on the damping is small and can be neglected. This means that for the acoustic analysis there is actually no need to determine the flow distribution in the filter. Flow effects can be neglected and the flow is only important for the estimation of the quadratic pressure drop at the outlet side (see Eq. (28)). Concerning the exact temperature distribution tests show that a very good approximation for the damping, the error is typically around 0.3 dB, is obtained by using a constant temperature equal to the average. A large effect of soot loading on the filter damping is also observed, which of course is related to a pressure drop increase due to the soot layer.

3. Measurements and model validation

3.1. Pressure drop measurements

The clean filter units tested were all mounted in 150 mm steel pipes which were connected to the flow test rig at the Marcus Wallenberg Laboratory, see Fig. 9. The pressure drop across the filters was measured using an electronic manometer (Swema Air 300), the average flow speed before the filter was measured using a pitot-tube connected to the same manometer and fixed at $2.5D$ from the inlet of the filter. The filter was fixed at a distance of $20D$ from the diverging conical part

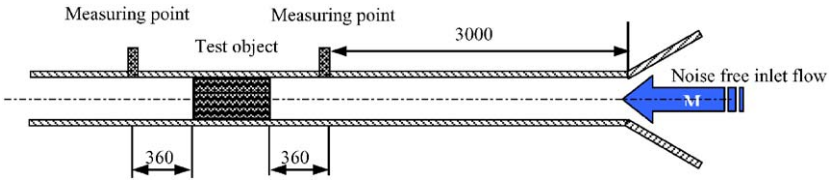

Fig. 9. Layout of the test rig for measurement of the filter pressure drop.

Table 2
Data for the tested DPF units including the flow loss coefficients (at 20 °C) determined from the pressure drop measurements

Filter name	Channel width $d_h \times 10^3$ (m)	Wall thickness $h_t \times 10^4$ (m)	Permeability $\sigma_w \times 10^{13}$ (m^2)	$n \times 10^{-5}$ (channels/m^2)	R_1 (Ns/m^3)	R_2 (Ns^2/m^4)
EX 200/14	1.44	3.55	2.5	3.10	184.1	39.2
EX 100/17	2.11	4.30	2.5	1.55	199.8	30.9
RC 200/12	1.50	3.04	25	3.87	87.1	29.2
RC 200/20	1.30	5.08	25	2.48	233.3	41.6

connected to a pressure chamber, where D is the diameter of the steel pipe. Fluctuations in the pressure measurements at the filter were typically ± 1 Pas.

Four different filters were tested; they all had the length 250 mm and the codes EX80: (200/14); EX80: (100/17); RC: (200/12), and RC: (200/20) where (x/y) stands for the number of cells per square inch/wall thickness in inch multiplied by 1000. A summary of the data for the filters is presented in Table 2.

The filters were tested for flow speeds up to 15 m/s and for every flow speed the filter pressure drop was measured twice, first with the flow rate increasing and then with the flow rate decreasing. Careful attention was paid to prevent and detect any leakage from the entrance and exit of the filters. To avoid leakage in the system the pressure drop measurements were made close to the filters, and seals were used for the ducts sections. A plot of the filter pressure drop data versus flow speed is shown in Fig. 10. The constants R_1 and R_2 in Eq. (1) were calculated based on a least-squares procedure and the results are summarized in Table 2.

The data in Table 2 is used for the predictions with the lumped impedance model in Section 3.2. It can be noticed that the linear flow coefficient (R_1) can be related to the wall resistance (R_w) and the laminar pressure drop through channels [2,4] via

$$R_w = 4R_1 d_{h1} LN/A. \tag{28}$$

The quadratic (R_2) flow coefficient is related to flow separation at the inlet/outlet sections and "turbulent" channel flow [2,4]. Typical Reynolds numbers at the inlet/outlet of the filters (based on channel width) for the tests reported here are 2000–4000, i.e., above the critical value. This implies that a turbulent flow exists at least in a part of the inlet/outlet channels. But since the flow

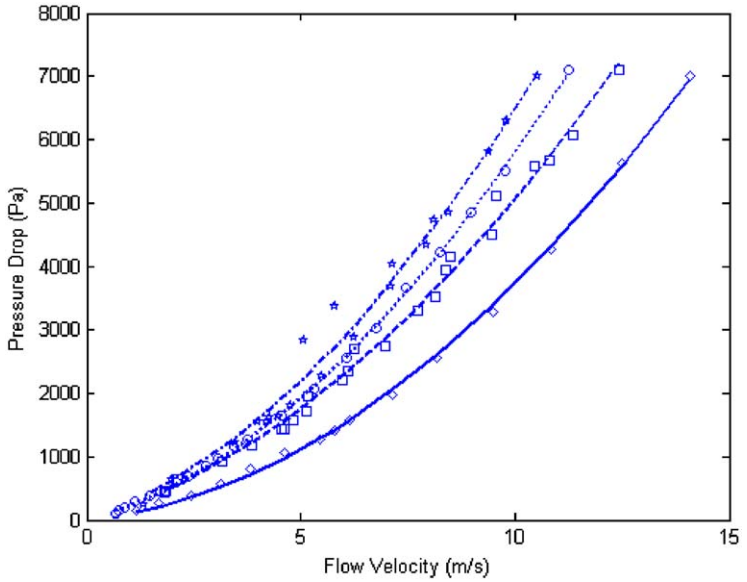

Fig. 10. Mean-flow velocity versus pressure drop (at 20 °C) for various types of clean filters. ∗ ∗ ∗, Measured (200/20); -.-., best fit for (200/20); ○ ○ ○, measured (200/14), ..., best fit for (200/14); □ □ □, measured (100/17); - - - -, best fit for (100/17); ◇ ◇ ◇, measured (200/12); —, best fit for (200/12).

speed exhibits a decrease along the inlet channels and increase along the outlet channels, due to the flow through the porous walls, there is also a laminar flow section. At operating conditions and with (say) a temperature of 500 °C the kinematic viscosity (assuming unchanged static pressure) will increase with a factor close to 4. The Reynolds number at the inlet/outlet sections will then decrease to values in the range 500–1000. This means that laminar flow will exist everywhere in the channels and the only possible quadratic pressure drop comes from flow separation at the inlet and outlet openings. Assuming an incompressible mean flow this implies [12]

$$R_2 = \begin{cases} \rho_{\mathrm{IN}}(1 - 1/m_{\mathrm{IN}})^2/4, \\ \rho_{\mathrm{OUT}}(1 - 1/m_{\mathrm{OUT}})^2/2, \end{cases} \tag{29}$$

where m_{IN} and m_{OUT} is the open area ratio at the inlet and outlet, respectively.

In the 1-D wave model this flow related loss is included by putting: $r_X = 2R_2U/A$ in Eq. (25), where X corresponds to IN + I or III + OUT and U equals the flow speed at the IN or OUT section respectively. The result in Eq. (29) implies that the total quadratic pressure drop coefficient (R_2) will be of the order 2–3 $\mathrm{Ns}^2/\mathrm{m}^4$ for the hot case, which compared to the values measured at cold conditions is a significant reduction. In practice this implies that there will be much weaker flow dependence for the filter damping at operating conditions as compared to the cold (20 °C) case.

3.2. Nonlinear effects

The highest sound levels will exist at the lowest engine harmonics (< 100 Hz) where the filter can be seen as a lumped resistive element. Assuming linear plane waves at the inlet and outlet side and

modeling the filter response via Darcy's law with Forschheimer's extension, Eq. (1), the effect of the quadratic filter response can be investigated. Based on the data presented in Table 2 valid for cold conditions (20 °C), it was found that nonlinear effects were negligible up to incident sound levels of 150 dB. As noted above at hot conditions the quadratic term will be significantly reduced, which implies that under real operating conditions the effect of local nonlinearities at a DPF should be small.

3.3. Comparison between measured and calculated transmission loss

The acoustic two-ports were also measured for the filter units defined in Table 2. The test rig for the pressure drop measurements was modified as shown in Fig. 11. Eight loudspeakers were used as acoustic sources equally divided between the upstream and downstream side. Two dissipative silencers were used one up and one down stream to reduce the effects of standing waves in the measurements. Fluctuating pressures were measured using six-condenser microphones (Brüel & Kjaer 1/4-inch 4938) flush mounted in the duct wall. Measurements were carried out in the plane wave range (0–1250 Hz) with a stepped-sine signal and flow noise suppression was done by correlation with the loudspeaker voltage. The two-port matrix was determined using the so-called source switching technique as described in Ref. [13].

In Figs. 12–15 transmission loss calculated from the measured two-port data is presented for a Mach number corresponding to a typical operating condition. In the figures predictions based both on the lumped impedance model and the 1-D wave model are shown. Concerning the lumped model the input for the calculations are the measured pressure drop data from Table 2. Concerning the 1-D wave model the wall resistance for the filters is calculated using the data in Table 2 and Eq. (9). For this cold case (20 °C) the speed of sound and the damping in the channels was assumed to follow case (ii) (see Section 2.2.1.2). As an alternative the total viscous damping from the walls was estimated by the measured linear pressure drop coefficient (R_1) using Eq. (28). This was combined with the adiabatic speed of sound (as in case (ii)) and $\alpha_j = 0$ in Eq. (7). To estimate the flow related losses at the inlet and outlet (see Eq. (25)) the following formula is proposed

$$r_{\mathrm{I+IN}} = r_{\mathrm{III+OUT}} = R_2 U_0 / A, \tag{30}$$

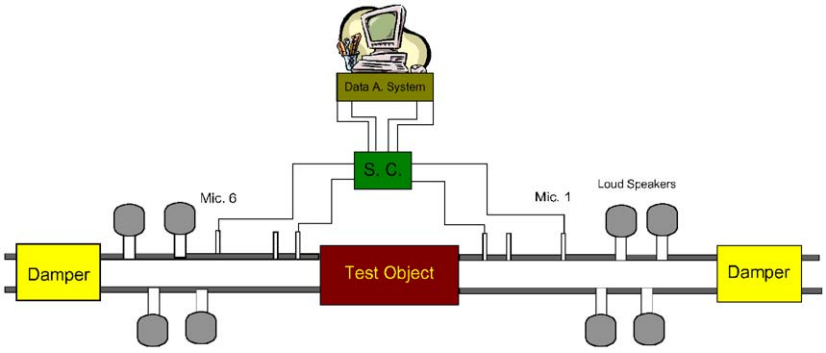

Fig. 11. Layout of the MWL test rig for determination of acoustic two-port data.

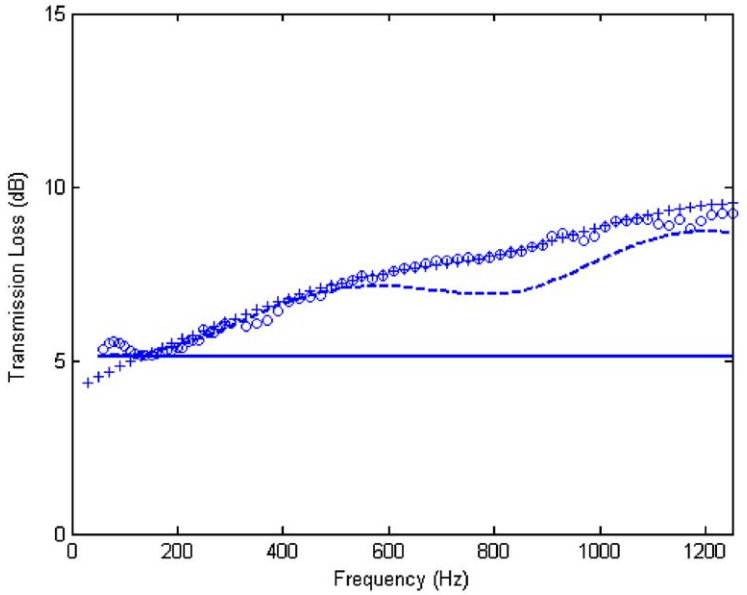

Fig. 12. Measured and predicted transmission loss for the (EX200/14) filter with $M = 0.02$ at the filter inlet. ○ ○ ○, Measured; —, predicted using lumped model; - - - -, predicted using 1-D model with measured wall resistance; + + +, predicted using 1-D model (case (ii)).

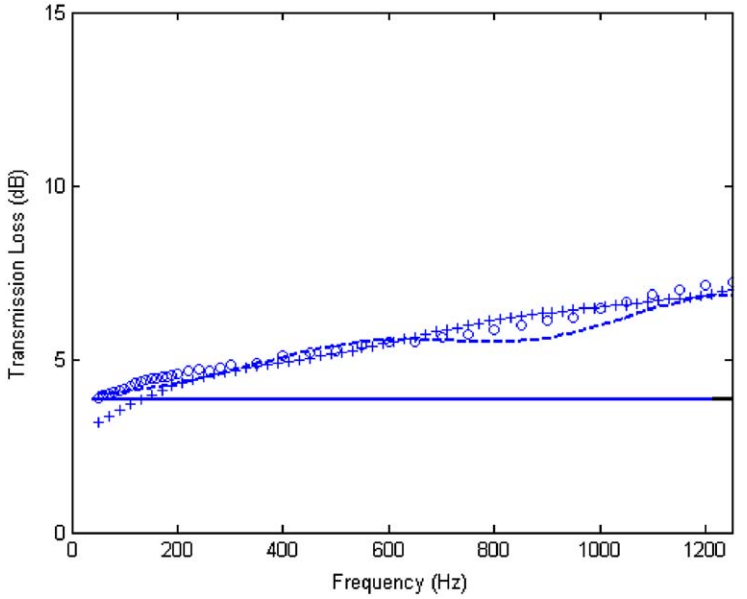

Fig. 13. Measured and predicted transmission loss for the (RC200/12) filter with $M = 0.015$ at the filter inlet. ○ ○ ○, Measured; —, predicted using lumped model; - - - -, predicted using 1-D model with measured wall resistance; + + +, predicted using 1-D model (case (ii)).

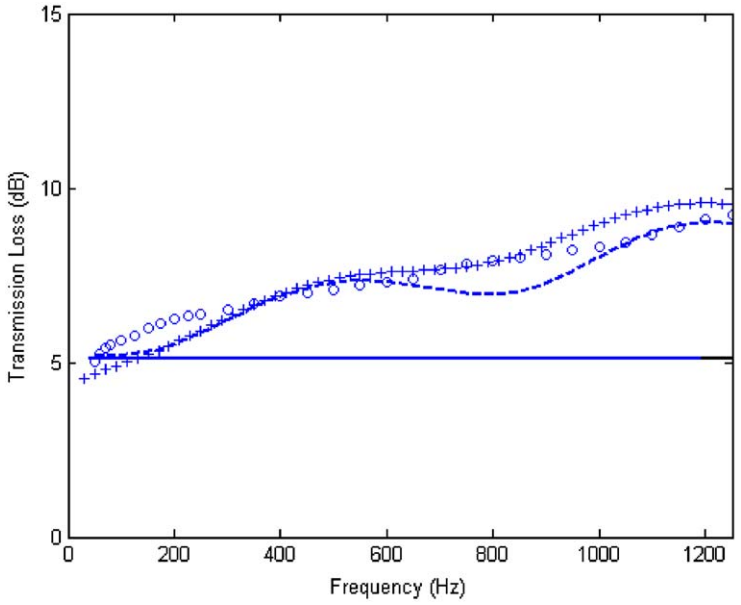

Fig. 14. Measured and predicted transmission loss for the (EX100/17) filter with $M = 0.020$ at the filter inlet. ○ ○ ○, Measured; —, predicted using lumped model; - - - -, predicted using 1-D model with measured wall resistance; + + +, predicted using 1-D model (case (ii)).

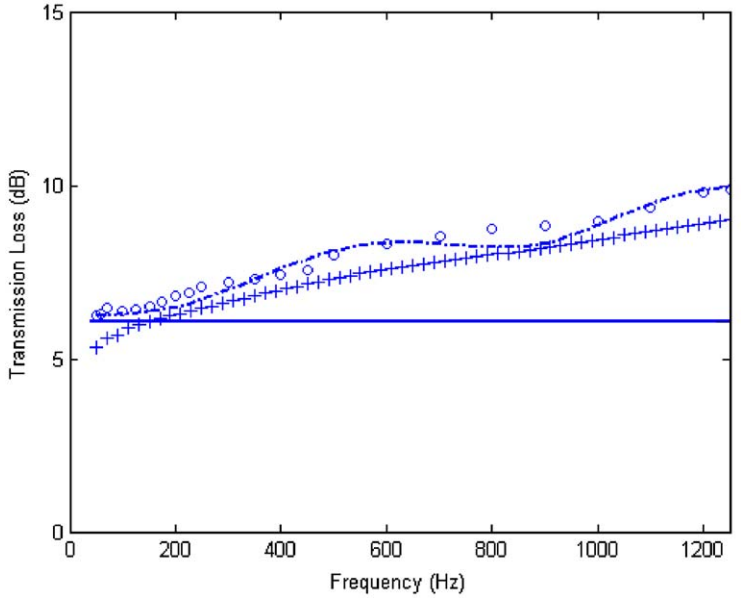

Fig. 15. Measured and predicted transmission loss for the (RC200/20) filter with $M = 0.021$ at the filter inlet. ○ ○ ○, Measured; —, predicted using lumped model; - - - -, predicted using 1-D model with measured wall resistance; predicted using 1-D model (case (ii)).

where it is assumed that the losses are equally distributed between the in- and outlet. This formula means that the quadratic flow loss is modeled as a lumped acoustic resistance, i.e., that it occupies a region that is acoustically compact.

As can be seen from Figs. 12–15 the agreement for the lumped model is satisfactory up to 200–300 Hz. The 1-D model using the case (ii) assumptions to estimate the speed of sound and damping agrees well with the measured data, except at low frequencies (<200 Hz). The 1-D model using the experimentally determined wall resistance values shows a better agreement for low frequencies, but becomes oscillating for higher frequencies.

4. Results and discussion

Two different models for calculating the acoustic two-port of diesel particulate filters have been presented. The models have been compared with experimental data and the agreement is satisfactory. The 1-D wave model (Section 2.2) works in the entire plane wave range and the simple lumped model (Section 2.1) works up to 200–300 Hz. Under real hot conditions this would mean 400–600 Hz. To continue the work and improve the 1-D model the acoustic damping along narrow channels with porous walls should be investigated further. Also measurements at hot conditions are necessary to finally validate the 1-D model and to check for instance if chemical reactions (a slow burning of soot) will influence the behavior.

Acknowledgements

The authors would like to thank Mikael Karlsson and William Easterling at SWENOX for supporting this work and for supplying filters for the testing. Financial support from the EC-project ARTEMIS (G3RD-CT-2001-00511) is also acknowledged as well as support from the ARTEMIS partner FAURICIA.

References

[1] M. Stamatelos, A review of the effect of particulate traps on the efficiency of vehicle diesel engines, *Energy Conversion Management* 38 (1) (1997) 83–99.
[2] A.G. Konstandopoulos, J.H. Johnson, Wall-flow diesel particulate filters-their pressure drop and collection efficiency, SAE Technical paper No. 890405, 1989.
[3] Konstandopoulos, M. Kostoglou, E. Skaperdas, Fundamental studies of diesel particulate filters: transient loading, Regeneration and Aging, SAE Technical paper 2000-01-1016, 2000.
[4] M. Masoudi, U. Zink, P. Then, D. Thompson, A. Heibe, Predicting pressure drop of ceramic wall-flow diesel particulate filters—theory and experiment, SAE Technical paper 2000-01-0184, 2000.
[5] S. Allam, M. Åbom, On acoustic modeling and testing of diesel particulate filters, *Proceedings of Inter-Noise Conference*, paper 250, 2002.
[6] J.H.M. Disselhorst, L. van Wijngarden, Flow in the exit of pipes during acoustic resonance, *Journal of Fluid Mechanics* 99 (1980) 293–319.
[7] P. Forchheimer, Wasserbewegung durch Boden, *Zeitschrift des VDI* 50 (1901).

[8] A.D. Pierce, *ACOUSTICS: An Introduction to Its Physical Principles and Applications*, second ed., Acoustical Society of America, New York, 1991.
[9] P.O.A.L. Davies, Practical flow duct acoustics, *Journal of Sound and Vibration* 124 (1988) 91–115.
[10] M.L. Munjal, *Acoustics of Ducts and Mufflers*, Wiley, New York, 1987.
[11] S. Boij, Reflection of sound at area expansions in a flow duct, *Journal of Sound and Vibration* 260 (2003) 477–498.
[12] B. Eck, *Techniche Strömungslehre*, Springer, Berlin, 1981.
[13] M. Åbom, Measurement of the scattering matrix of acoustical two-ports, *Journal of Mechanical System and Signal Processing* 5 (1991) 89–104.